ARMY RESEARCH LABORATORY

Point-Scatterer Model for a Soviet T-62 Tank at 95 GHz

by Geoffrey H. Goldman

ARL-TR-612

April 1995

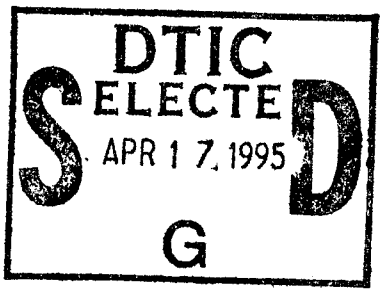

The findings in this report are not to be construed as an official Department of the Army position unless so designated by other authorized documents.

Citation of manufacturer's or trade names does not constitute an official endorsement or approval of the use thereof.

Destroy this report when it is no longer needed. Do not return it to the originator.

REPORT DOCUMENTATION PAGE

Form Approved
OMB No. 0704-0188

1. AGENCY USE ONLY *(Leave blank)*	2. REPORT DATE	3. REPORT TYPE AND DATES COVERED
	April 1995	Final, January to December 1991

4. TITLE AND SUBTITLE
Point-Scatterer Model for a Soviet T-62 Tank at 95 GHz

5. FUNDING NUMBERS
PE: 62120.AH16

6. AUTHOR(S)
Geoffrey H. Goldman

7. PERFORMING ORGANIZATION NAME(S) AND ADDRESS(ES)
U.S. Army Research Laboratory
Attn: AMSRL-SS-SD
2800 Powder Mill Road
Adelphi, MD 20783

8. PERFORMING ORGANIZATION REPORT NUMBER
ARL-TR-612

9. SPONSORING/MONITORING AGENCY NAME(S) AND ADDRESS(ES)
U.S. Army Research Laboratory
2800 Powder Mill Road
Adelphi, MD 20783

10. SPONSORING/MONITORING AGENCY REPORT NUMBER

11. SUPPLEMENTARY NOTES
AMS code: 622120.H16
ARL PR: 51E21A

12a. DISTRIBUTION/AVAILABILITY STATEMENT
Approved for public release; distribution unlimited.

12b. DISTRIBUTION CODE

13. ABSTRACT *(Maximum 200 words)*

A simulation program based on an isotropic point-scatterer model was used to reconstruct 95-GHz, monopulse radar measurements of a T-62 Soviet tank taken with the target on a rotating turntable at a 60° radar depression angle and at a range of 95 m. Scattering centers were generated from three-dimensional inverse synthetic aperture radar (ISAR) images, which had a resolution of approximately 0.23 m in downrange, 0.21 m in crossrange, and 0.1 m in elevation. Model- and measurement-based radar cross-section (RCS) and azimuth and elevation aimpoint calculations were compared for 1° target azimuth intervals over 360°. The agreement and the precision of measured and simulated values were evaluated.

Simulation values approached an asymptotic level of maximum agreement with measured values when target models were used in the simulation program that contained a minimum of 40 scattering centers and an average of 68 scattering centers. This resulted in an agreement in the RCS mean values of approximately 0.04 ± 0.6 dB and in the mean azimuth and elevation aimpoint values of less than

(continued on next page)

14. SUBJECT TERMS
Millimeter wave, radar, target model

15. NUMBER OF PAGES
33

16. PRICE CODE

17. SECURITY CLASSIFICATION OF REPORT	18. SECURITY CLASSIFICATION OF THIS PAGE	19. SECURITY CLASSIFICATION OF ABSTRACT	20. LIMITATION OF ABSTRACT
Unclassified	Unclassified	Unclassified	UL

NSN 7540-01-280-5500

Standard Form 298 (Rev. 2-89)
Prescribed by ANSI Std. Z39-18
298-102

13. Abstract (cont'd)

0.01 ± 0.11°. The statistical agreement between measured and simulation values was also evaluated with nonparametric statistical tests performed at a 95-percent level of confidence. The percentage-passed rates for a distribution and a median value test were 58 and 66 percent, respectively. An error analysis of these results revealed that the discrepancies between measured and simulation values were caused by a lack of information on the exact phase relationships between the scattering centers. Overall, the agreement between measurement- and model-based RCS and aimpoint calculations was good.

Contents

Figures

Tables

1. Introduction

Validated and computationally efficient target models are needed for evaluating millimeter-wave seeker design. A simple modeling technique is to use a statistical distribution to describe target features such as radar cross section (RCS). This technique requires a minimal amount of processing time, but it is usually too imprecise for modeling tasks such as evaluating smart munitions performance. A more complex model involves the use of the physical geometry of the target, with ray-tracing techniques used to simulate radar returns. The validity of this technique is higher, but it requires a large amount of processing, which makes it inappropriate for some applications. A less computationally intensive technique with potentially high validity is the use of a point-scatterer model, which is usually generated from precise radar measurements of a target.

Point-scatterer models characterize a target at a specific aspect angle by a list of scattering centers. Intuitively, the scattering centers represent the areas on a target that are responsible for radar returns. They consist of a three-dimensional (3-D) location, amplitude, and sometimes a phase offset. Scattering centers are usually derived from 3-D inverse synthetic aperture radar (ISAR) images of a target or from 2-D ISAR images with the third dimension derived from their projection onto the physical geometry of the target. One generates simulated target signatures by computing the coherent sum of the radar radiation reflected by scattering centers that have been rotated and translated so that their location with respect to the radar corresponds to the particular aspect angle and range of the target being modeled. A new set of scatterer centers is required after some small angular change in the orientation of the target.

Point-scatterer models are typically employed to predict the RCS and glint (tracking-angle scintillation) for military targets. Several programs have made such predictions using specific target, seeker, and modeling parameters [1–4]. The objectives of this report are similar: I evaluate an isotropic point-scatterer modeling technique using 95-GHz monopulse radar measurements of a Soviet-built T-62 tank by analyzing the tradeoffs between model computer simulation time and the degree of model validity and by assessing the relative errors associated with the model- and measurement-based RCS and tracking aimpoint calculations. Positive evaluation test results will validate the use of the model-generated scattering centers for missile flight simulation software and hardware-in-the-loop simulators.

In the following sections, I describe how the model was constructed and explain the evaluation testing criteria. In the results section, I evaluate the performance of the model, and summarize the important outcomes in the conclusion section.

2. Procedure

2.1 Generation of Scattering Centers

Scattering centers for the target model were derived from data obtained by Harry Diamond Laboratories (HDL)* at the Russell Tower on Redstone Arsenal in 1989 [5,6]. A two-component, amplitude-comparison monopulse instrumentation radar was used to make coherent measurements of a Soviet-built T-62 tank at a 60° radar depression angle while it was rotating on a turntable from 0° to 360° azimuth. The range from the radar to the target was approximately 95 m. A ramp of data (64 radar pulses of 100-ns duration, frequency-stepped in 10-MHz intervals between 95.0 and 95.63 GHz) was sampled every 0.0131° azimuth for a given polarization. The signal-to-clutter ratio was estimated to be between 15 and 25 dB, depending on the orientation of the target. The signal-to-noise ratio was much higher. ISAR images of the target were generated from 64 ramps of data obtained with right-hand transmitted, right-hand received (RR) circular polarization for every target azimuth interval of approximately 0.84°.

The processing performed to generate 3-D ISAR images from the data consisted of applying a filter, a fast Fourier transform (FFT), a translation in azimuth, an antenna pattern shape compensation, and a turntable RCS reduction algorithm [7]. First, 64 consecutive ramps of data measured with the monopulse radar sum and elevation-difference channel were smoothed with a 2-D Kaiser filter with 25-dB sidelobes. Next, 64-by-64 2-D FFTs were applied, and the resulting sum and elevation channel ISAR images were shifted by an empirically calculated azimuth angle offset. This shift was required to align the center of the images with the radar boresight position. Then, the sum channel ISAR image was divided by the sum channel antenna pattern of the radar (see the appendix). To reduce the likelihood of clutter at the edges of an ISAR image being incorrectly interpreted as scattering centers, I limited the maximum antenna pattern correction to 3 dB. The resulting 2-D sum channel ISAR image was used in the calculation of the downrange positions, crossrange positions, and amplitudes of the scattering centers. Figure 1 shows an example of a 2-D ISAR image with a T-62 tank outline superimposed.

The elevation positions of the scattering centers were calculated from the ratio of the elevation-difference channel to sum channel ISAR image of the target [8]. This resulted in a 3-D ISAR image that had a resolution of approximately 0.23 m in downrange, 0.21 m in crossrange, and 0.1 m in elevation. Any point-scatterers determined to have an elevation position more than 3.5 m below the ISAR image plane were eliminated. (These scatterers were probably caused by reflections from the turntable apparatus.) Because the resolution of the ISAR images was insufficient for the position of the scattering centers to be determined to within a radar wavelength, a random position offset between 0 and the wavelength of the radar was

*Now part of the U.S. Army Research Laboratory (ARL).

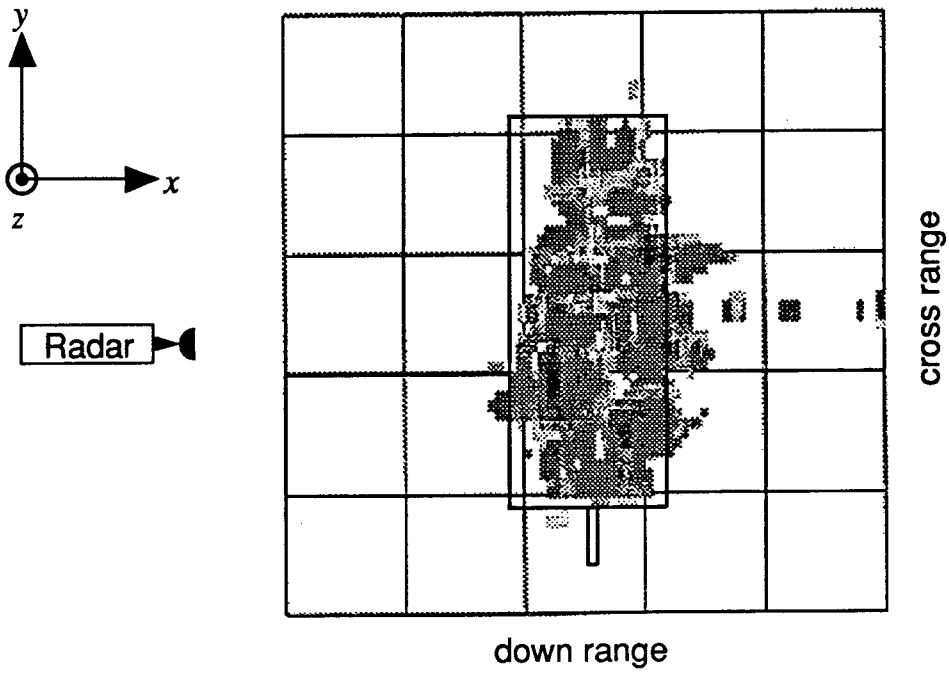

Figure 1. ISAR image of a T-62 tank for 60° radar depression angle, 270° target azimuth angle, and RR polarization. Radar is positioned at origin of coordinate system.

associated with each scattering center. The average position of the ISAR resolution cell was not used, because this could result in the model calculations generating unnatural interference patterns.

The amplitudes and the coordinates of the target scattering centers were determined from 3-D ISAR images by a scatterer selection criterion with two adjustable parameters: minimum ISAR RCS percentage and minimum number of scatterers. First, the total RCS of an ISAR image was computed by the summing of the RCS (in square meters) associated with each cell over all ISAR resolution cells (64×64). Next, the RCSs of the ISAR resolution cells were sorted according to their magnitude, and the largest scatterers were accumulated and summed until their combined RCS exceeded a selected percentage of the total ISAR RCS. If the total number of cells accumulated was less than a selected minimum number, additional cells were selected until that number was reached. Once the number of cells selected was determined, the RCSs of these scattering centers were normalized so that their sum equaled the total RCS of the original ISAR image. For this normalization, a fixed offset (in decibels) was added to the magnitude of the RCS of each cell selected, and the value of the sum was assigned to a scattering center. Table 1 shows each scatterer selection criterion that was evaluated. Associated with each minimum-ISAR-RCS-percentage parameter is a corresponding minimum-number-of-scatterers parameter that for brevity I do not often restate in the text. For example, the 70-percent-scatterer-selection criterion has an implied minimum of 40 scattering centers associated with it. I chose the scatterer selection criterion parameters with the intent of modeling all aspect angles of the target with equal validity, rather than to fulfill an equal simulation processing-time requirement.

Table 1. Scatterer selection criterion chosen for evaluation of point-scatterer model.

Minumum ISAR RCS percentage	Minimum number of scatterers
20	6
30	10
40	15
50	20
60	25
70	40
80	70
90	100

I applied the point-scatterer model by coherently summing the electromagnetic radiation reflected by each scattering center associated with a particular target orientation when the target was illuminated by radiation with a specific pattern. The resulting electric field is calculated from

$$E_{i,q}(f) = \sum_{s=1}^{S} A_s e^{j\phi_s(f)} G_c\left(\theta_{az_s}, \theta_{el_s}\right) , \tag{1}$$

where E = electric field, i = in-phase component, q = quadrature component, f = frequency of transmitted radiation, s = scatterer index number, S = total number of the scatterers, A_s = amplitude of the sth scattering center, j = complex number, $\phi_s(f)$ = phase of the electric field resulting from the sth scattering center for the fth frequency, G_c = antenna pattern for a particular monopulse channel (see the appendix), θ_{az} = azimuth angle, and θ_{el} = elevation angle [9]. The phase of the electric field, $\phi_s(f)$, is given by

$$\phi_s(f) = 4\pi\left[\frac{\left(x_s^2 + y_s^2 + z_s^2\right)^{1/2}}{\lambda_f}\right] + \frac{\lambda_0 \theta_{rand_s}}{\lambda_f} , \tag{2}$$

where x_s, y_s, and z_s are the downrange, cross range, and elevation position of the sth scatterer with respect to the radar, θ_{rand_s} = random phase offset uniformly distributed between 0 and 2π, λ_0 = wavelength of the center frequency, and λ_f = transmitted wavelength, which is a function of f = frequency. We can determine $\phi_s(f)$ by dividing the path length from the radar to the scattering center and back by the wavelength of the transmitted radiation and multiplying by 2π, and then add random position offset.

The multiplication of the random phase offset by a frequency-dependent scale factor results in the second term in equation (2) being equivalent to a random position offset chosen between 0 and the wavelength of radar for the middle radar wavelength. These equations assume that the scatterers are isotropic reflectors, that there is no multipoint scattering, and that the scattering centers of the target are in the far field of the radar.

The simulation program reconstructed monopulse radar returns from point-scatterer target models. I performed model calculations by applying equations (1) and (2) to a set of scattering centers using the sum- and difference-channel antenna patterns and 64 frequencies that corresponded with the characteristics of ARL's instrumentation radar. Initially, a set of target-scattering centers, derived from a 3-D ISAR image for a particular target orientation, was rotated 0.419° counterclockwise with respect to the turntable and assigned a random phase between 0 and 2π. The random phases were converted to random position offsets (see eq (2)). Next, the scattering centers were incrementally rotated 0.0131° clockwise, and model calculations were performed after each rotation. This process continued until the scattering centers were rotated through 0.84° azimuth, and 64 ramps of simulated data were generated. After this, a new set of scattering centers was required, and the entire process was repeated. The rotation scheme used in the simulation program attempted to match the model- and measurement-based calculations ramp for ramp. Approximately 75 consecutive ramps of measured or simulated data were contained in a 1° target azimuth interval.

2.2 Generation of RCS and Aimpoints

RCS and tracking aimpoint values were calculated from high-range-resolution (HRR) profiles created with a ramp of sum and difference channel data. The general processing performed to create an HRR profile consisted of smoothing each ramp of data with a Taylor window, padding, and performing a 128-point FFT [10]. Any cell in a sum channel HRR profile determined to have an elevation extent below –3.5 m was set to zero (this cell was probably caused by a reflection from the turntable apparatus). I calculated the RCS by summing the RCS value (in square meters) for each of the sum channel HRR bins, and then converting the RCS to units of dBsm. This calculation is equivalent to determining the RCS by averaging the magnitude of the radar target returns over frequency with the turntable RCS contribution reduced. I determined the peak RCS value in the sum channel HRR profile by selecting the HRR bin with the largest RCS value and subtracting from its RCS a fixed offset (in decibels), empirically calculated for each scatterer selection criterion. The offset was chosen to make the average modeled peak RCS equal to the average measured peak RCS. The RCS of the target is denoted "RCS sum" and the peak RCS is denoted "RCS peak" in the labels for the figures and tables.

Azimuth and elevation aimpoint tracking position or boresight errors were calculated from HRR profiles with an averaging and a peak algorithm. The averaging algorithm averaged together the ratios of the difference channel over the sum channel HRR profiles for all sum channel HRR bins that were within 15 dB of the HRR peak RCS, as shown by

$$\Gamma_{az} = \frac{1}{K} \sum_{k} \mathrm{Re}\left[\frac{\Delta_{az}(k)}{\Sigma(k)}\right], \tag{3}$$

$$\Gamma_{el} = \frac{1}{K}\sum_{k} \mathrm{Re}\left[\frac{\Delta_{el}(k)}{\Sigma(k)}\right], \tag{4}$$

where Δ_{az} and Δ_{el} represent the azimuth- and elevation-difference channel HRR profiles, Σ = sum channel HRR profile, and K = total number of the k bins selected [11]. The peak algorithm was also computed for equations (3) and (4) for $K = 1$ with the bin that contained the peak RCS. Once the average or peak ratio was computed, it was converted to an aimpoint angle through an antenna-pattern-based ratio look-up table.

2.3 Model Evaluation

The agreement between model- and measurement-based RCS and aimpoint calculations was evaluated statistically, quantitatively, and visually. The statistical analysis determined how often the measured and simulation (model-based) values were significantly different. The quantitative analysis determined the magnitude of differences, and the visual analysis was used to reveal any patterns or trends that could be missed by a strictly numerical analysis. For a visual evaluation of the agreement, the measured and simulation values were filtered through a 64-point moving average window, plotted, and "qualitatively studied." This window size was chosen to match the simulation program point-scatterer target model update rate of approximately 0.84°.

For a quantitative evaluation of the model, the standard deviation of the difference between the 1° average measured and 1° averaged simulation values was computed. First, measured and simulation values were separately averaged for 75 consecutive ramp intervals, or approximately a 1° target azimuth interval. New average values were computed every 38 ramps, approximately every 0.5° of azimuth, for the entire test interval. Next, their standard deviation was computed from

$$\sigma = \left[\frac{1}{K-1}\sum^{K}\left(\bar{x}_{meas_k} - \bar{x}_{sim_k} - \mu\right)^2\right]^{1/2}, \tag{5}$$

where σ = standard deviation, $\bar{x}$ = average of 75 consecutive measured or simulation values (designated by the subscripts *meas* or *sim*, respectively), μ = average difference between the means of x_{meas} and x_{sim}, and K = total number of test intervals.

For a statistical analysis of the agreement between measured and simulation values, a Kolmogorov-Smirnov (KS) test and a Wilcoxon signed rank (WSR) test for a paired experiment were also applied over identical 1° intervals every 0.5° at the 95-percent level of confidence [12,13]. These tests were chosen to correspond with criteria proposed by Saylor and Harrison [14].

A standard procedure for making statistical inferences is to accept a hypothesis called an alternative hypothesis (H_1) by rejecting its negation, the

null hypothesis (H_0). Because of the nature of the statistical tests selected, the desired result was the acceptance of the null hypotheses, which are mathematically described as

$$\text{(KS)} \quad H_0: P\left(X_{sim} \le a\right) = P\left(X_{meas} \le a\right) \text{ , for all } a \text{ ,}$$
$$\text{(WSR)} \quad H_0: d_{meas} - d_{sim} = 0.0 \text{ ,}$$

where P = the probability distribution function, X_{meas} = a measured random variable, X_{sim} = a simulation random variable, a is a dummy variable for the KS test, and d_{meas} = the median of X_{meas} and d_{sim} = the median of X_{sim} for the WSR test. Acceptance of the null hypothesis for the KS test determined that the measured and simulation values did not come from different probability distributions, or more simply put, they had identical probability distributions. Acceptance of the null hypothesis for the WSR test determined that the medians of the measured and simulation values were not different, or more simply put, the values had identical medians. This means, for example, that if the selected statistical tests were applied to data generated from two independent random variables sampled from identical probability distributions, the above null hypotheses would be accepted in approximately 95 percent of the trials.

2.4 Application of Model

The degree to which the model is valid is characterized by the results of the visual, quantitative, and statistical analysis. The improvement in model validity was examined as the number of scatterers was increased for a limited azimuth angle interval of the target. I selected a near-optimally valid scatterer selection criterion by determining when a large increase in the number of scatterers produced a very small increase in the validity of the model. In addition, I examined the precision of measured RCS and aimpoint values by comparing the agreement between two sets of measurements that were collected for identical azimuth angular regions of the target. I also examined the precision of the simulation values by comparing the agreement between two sets of simulation values calculated with scattering centers that were identical except for a different random position offset between 0 and the radar wavelength associated with each scattering center.

3. Results

3.1 Scatterer Selection Criteria

I evaluated target models generated with each scatterer selection criterion listed in table 1 to determine the tradeoffs between model validity and computer processing requirements. The amount of computer processing required to apply the point-scatterer model was directly proportional to the number of scatterers in the target model. The number of scatterers needed to satisfy the various scatterer selection criteria (given in table 1) was determined for four 10° target azimuth intervals, and are plotted in figure 2. The bottom curve of figure 2 also shows a plot of the minimum number of scatterers required for each ISAR-RCS-percentage value that was given in table 1. The curves in figure 2 show that the average number of scatterers selected increases exponentially with the minimum-ISAR-RCS-percentage parameter specified in the scatterer selection criteria.

Figure 2 also indicates that fewer scatterers were usually selected around the cardinal angles, 90° and 180° azimuth, than around the noncardinal angles, 135° and 155° azimuth. At cardinal angles, the ISAR image was often dominated by a few large scattering centers. Requiring a minimum number of scatterers often resulted in the specified percentage of the minimum ISAR RCS being exceeded. Figure 3 shows the resulting total ISAR RCS percentage for each scatterer selection criterion. As shown in the fig-

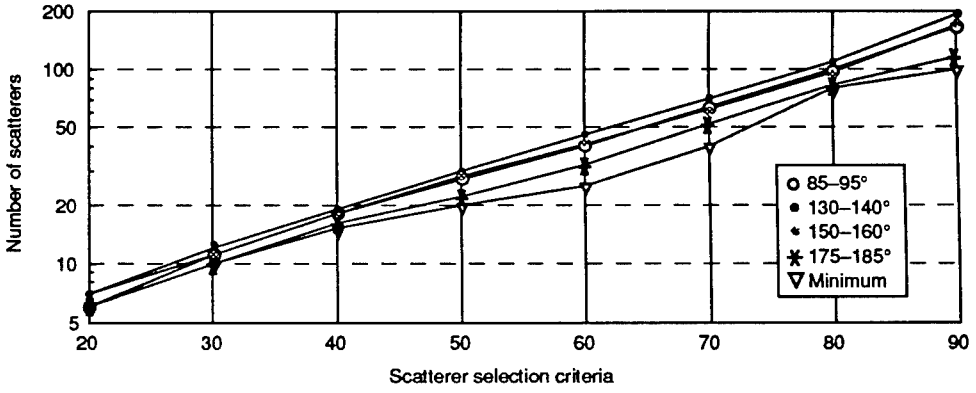

Figure 2. Average number of scattering centers selected to characterize four 10° azimuth intervals of a T-62 tank.

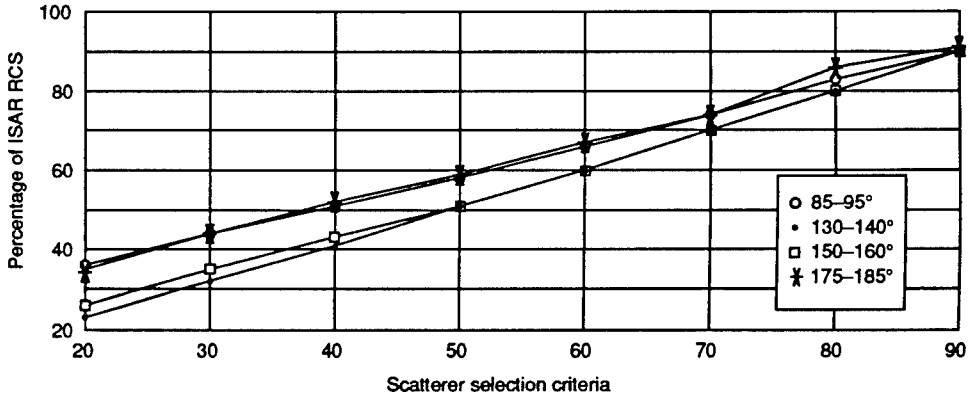

Figure 3. Average percentage of total ISAR RCS resulting when scatterer selection criteria are applied to four 10° azimuth intervals of a T-62 tank.

ure, the total ISAR RCS percentage for the target azimuth angles centered around the cardinal angles is significantly higher than for the target azimuth angles centered around the noncardinal angles, especially for the lower values of the ISAR-RCS-percentage parameter.

3.2 Model Optimization

I assessed the agreement between measurement- and model-based calculations for each scatterer selection criterion using the data for the same four 10° target azimuth intervals that were used to calculate the curves in figures 2 and 3. The agreement was evaluated visually, quantitatively, and statistically. Figures 4, 5, and 6 show a visual example of how the agreement for the RCS and the average azimuth- and elevation-aimpoint values varied with each scatterer selection criterion for the interval between 175° and 185° of target azimuth. These plots were smoothed with a 0.84° moving average window. This example indicates that for the azimuth and elevation aimpoint calculations, the more scattering centers used to characterize the target, the better the agreement between simulation and measured values, but the RCS agreement was optimal at the 50-percent-scatterer selection criterion. However, other regions of the target show that the improvement in the visual agreement levels off at various scatterer selection criteria.

Figures 7 and 8 show the results of the quantitative analysis. The agreement between measured and simulation RCS and aimpoint values was again evaluated for the four 10° target azimuth intervals listed in figures 2 and 3. The standard deviation of the difference between the 1° average of the measured values and that of the simulation values sampled every 0.5° was computed for each scatterer selection criterion. The lower the standard deviation, the better the agreement. Note that the mean value was not used as an indicator of model validity, because for most of the calculations performed, the expected difference between the measured and the simulation values theoretrically should be zero. The results for the RCS shown in figure 7 indicate that near-optimal agreement was obtained at the 50-percent-ISAR-RCS point. No significant reduction in the standard deviation was achieved after this point. The aimpoint results shown in figure 8 indicate that in most cases there was only a small reduction in the standard deviation after the 70-percent-ISAR-RCS point. These results indicate that near-optimal agreement between measured and simulation values could be obtained with those scatterers chosen with the 70-percent-scatterer selection criterion.

Figures 9 and 10 show the statistical analysis results for the agreement of RCS and aimpoint values evaluated for the four 10° intervals of data. KS and WSR tests were performed over 1° intervals of data every 0.5°. The higher the percentage-passed rate for these tests, the better the agreement between measured and simulation values. The test results show that there was considerable variability in the percentage-passed rates. To facilitate analysis of the overall trends in these figures, I averaged the RCS and aimpoint percentage-passed rates together and plotted them in figure 11.

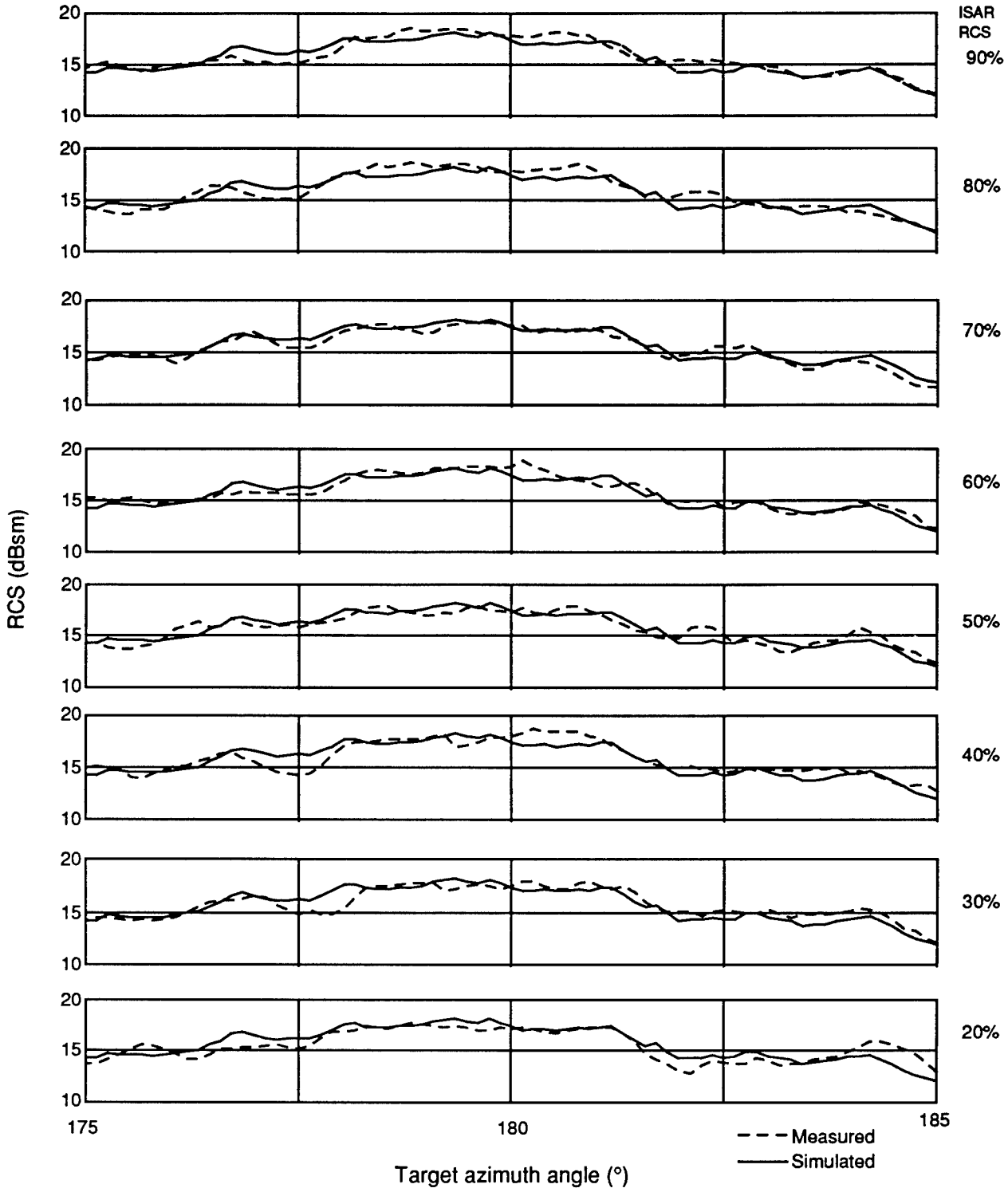

Figure 4. Measured and simulation RCS values smoothed with a 0.84° moving average window with simulation values calculated for each scatterer selection criterion.

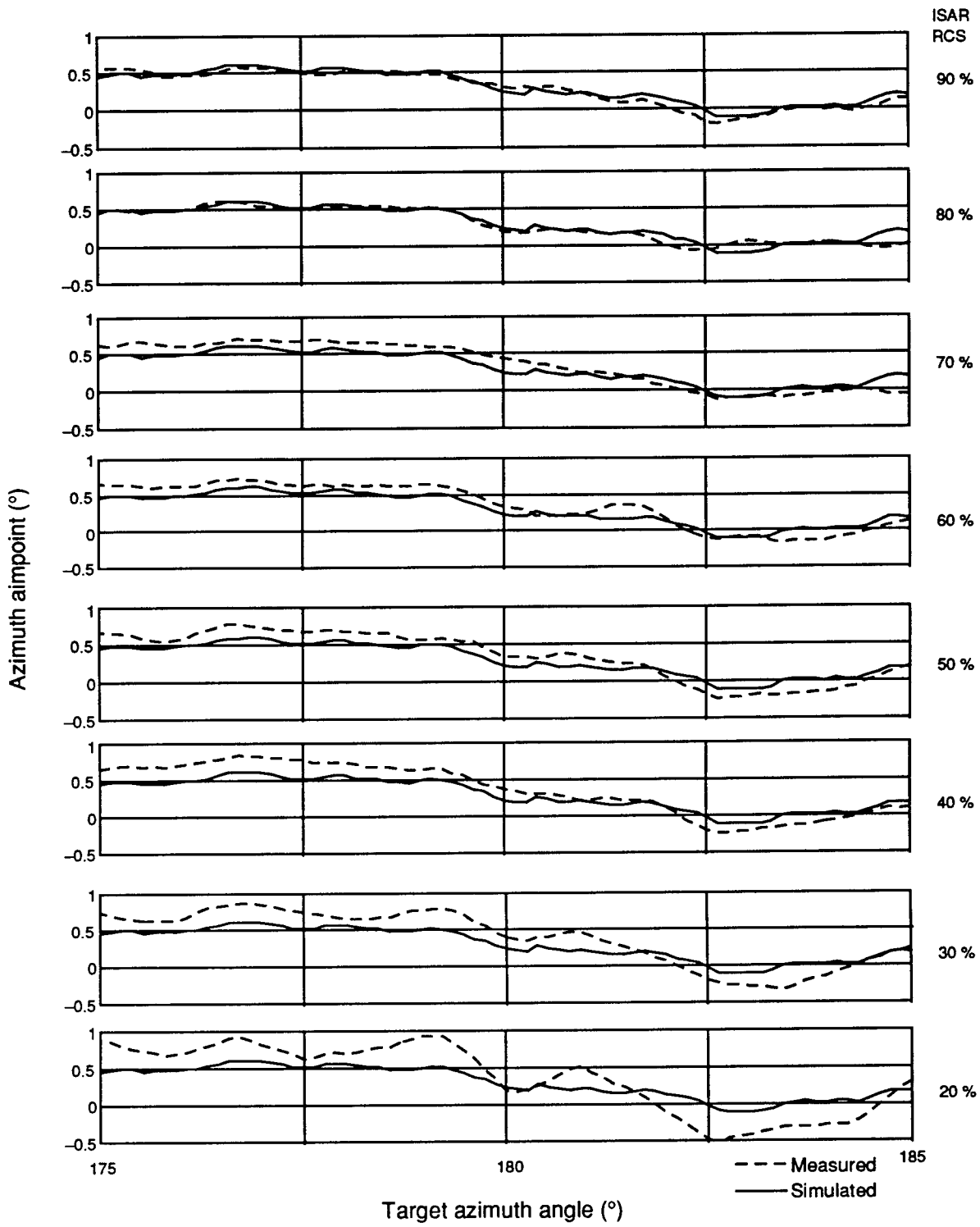

Figure 5. Measured and simulation average azimuth aimpoint values smoothed with a 0.84° moving average window with simulation values calculated for each scatterer selection criterion.

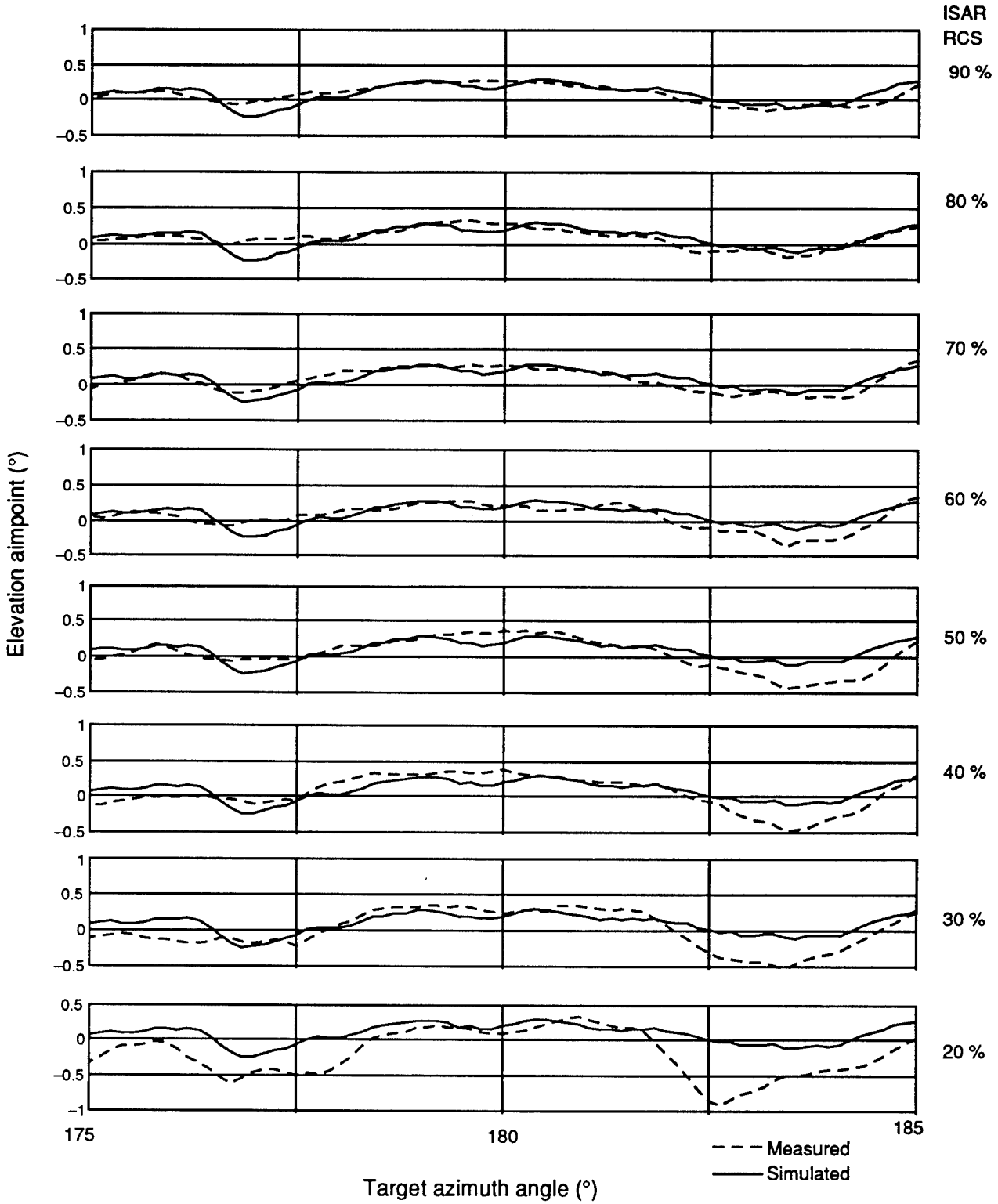

Figure 6. Measured and simulation average elevation aimpoint values smoothed with a 0.84° moving average window with simulation values calculated for each scatterer selection criterion.

Figure 7. Standard deviation of difference between measured and simulation RCS values averaged over 1° intervals for four 10° azimuth intervals of a T-62 tank.

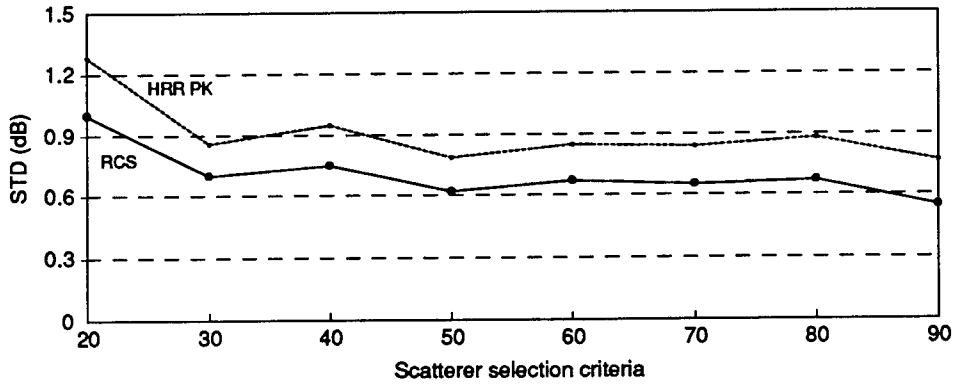

Figure 8. Standard deviation of difference between measured and simulation aimpoint values averaged over 1° intervals for four 10° azimuth intervals of a T-62 tank.

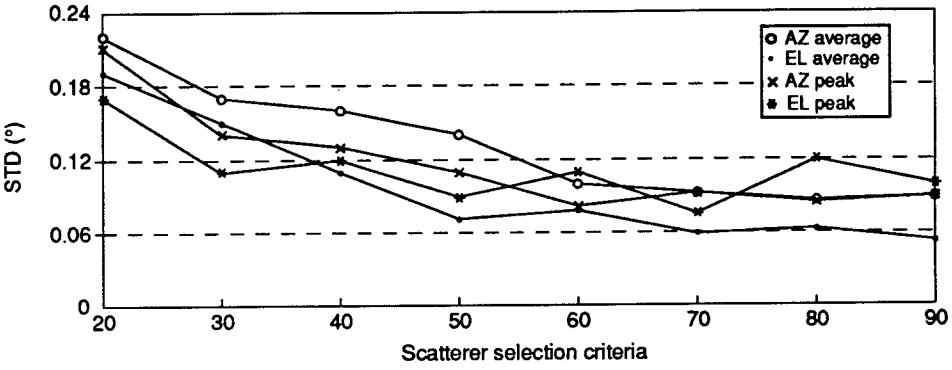

Figure 9. Wilcoxon signed rank statistical test results for RCS and aimpoint calculations for four 10° azimuth intervals of a T-62 tank.

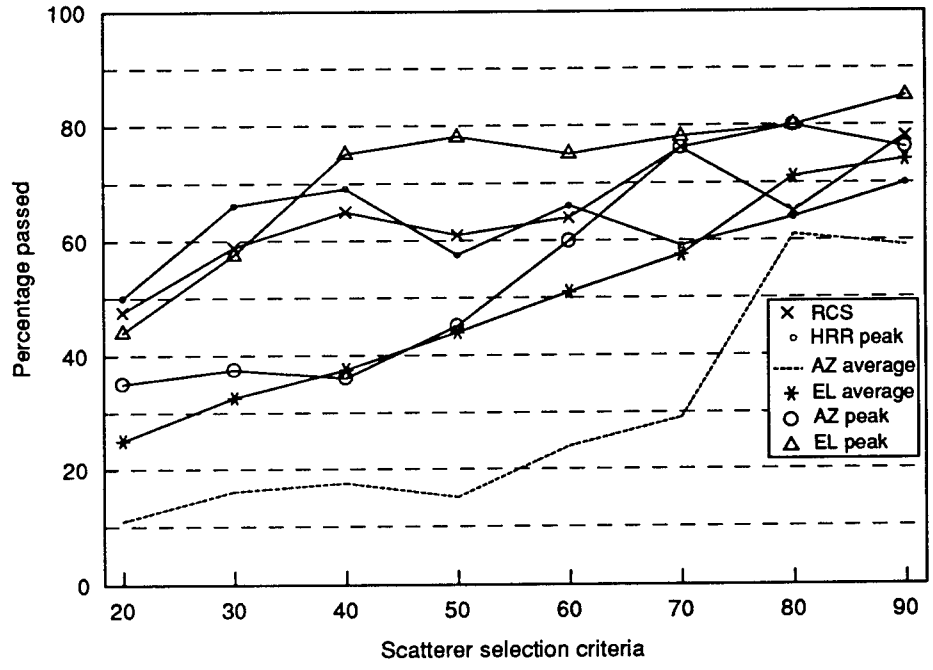

Figure 10. Kolmogorov-Smirnov statistical test results for RCS and aimpoint calculations for four 10° azimuth intervals of a T-62 tank.

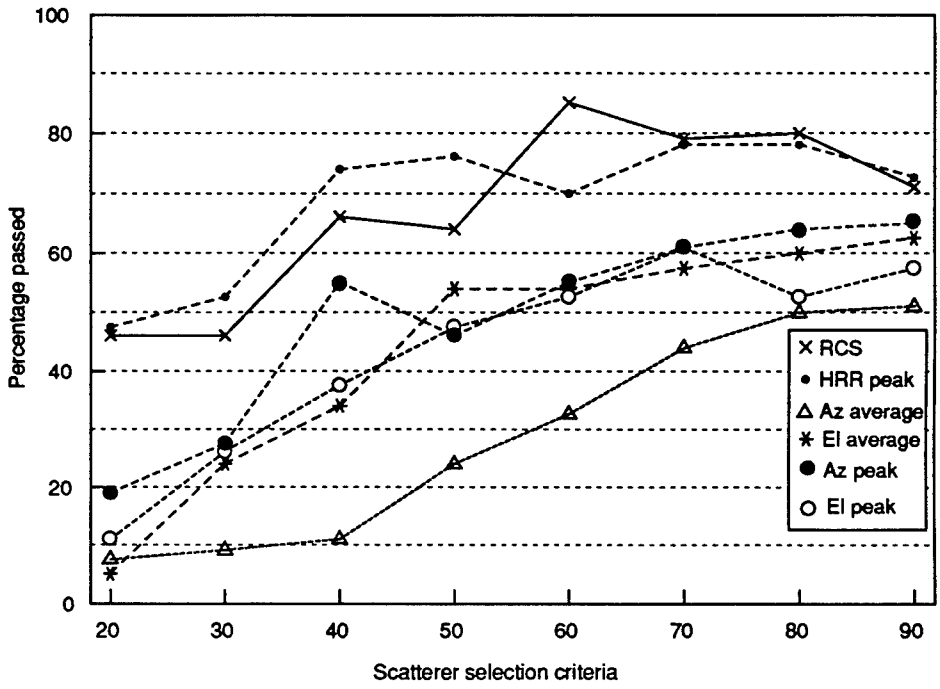

Figure 11. Average statistical test results for four 10° azimuth intervals of a T-62 tank.

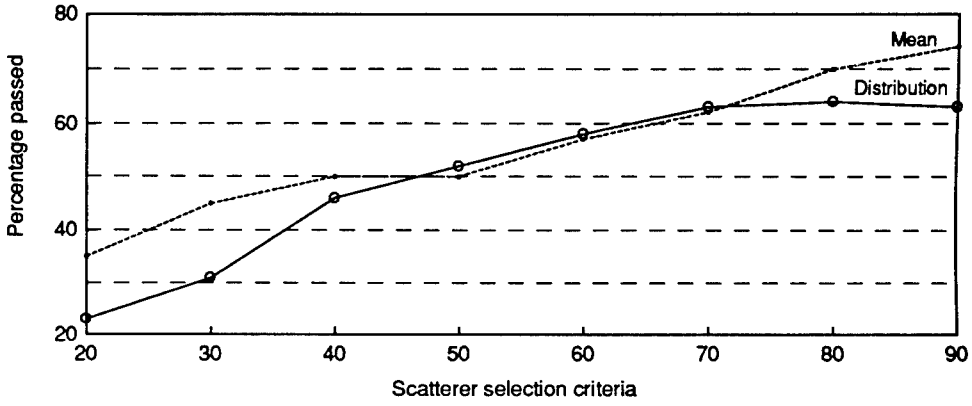

These results show that for the WSR test, there was no convergence to an optimal percentage-passed rate for a certain scatterer selection criterion. However, the KS test results indicate that a near-optimal percentage-passed rate was obtained at the 70-percent-ISAR-RCS point.

One can use the results presented in this section to estimate the average number of scatterers required to characterize a target for an application with a specific model validity requirement. They indicate that close to optimal agreement can be obtained if one chooses the scatterer selection criterion that requires a minimum of 70 percent of total ISAR RCS and a minimum of 40 scatterers. Although slightly greater model validity can be achieved, attaining it would result in an exponential increase in the number of scattering centers (as shown in fig. 2) and in the amount of computer processing required.

3.3 Model Evaluation

The simulation program was executed for the full 0° to 360° range of target azimuth angles with target models generated by the 70-percent-scatterer selection criterion. This criterion resulted in models with an average of 68 scatterers and 71 percent of the total ISAR RCS. The visual agreement between measured and simulation values can be seen from the curves in figure 12. The values were smoothed with a 0.84° moving average window

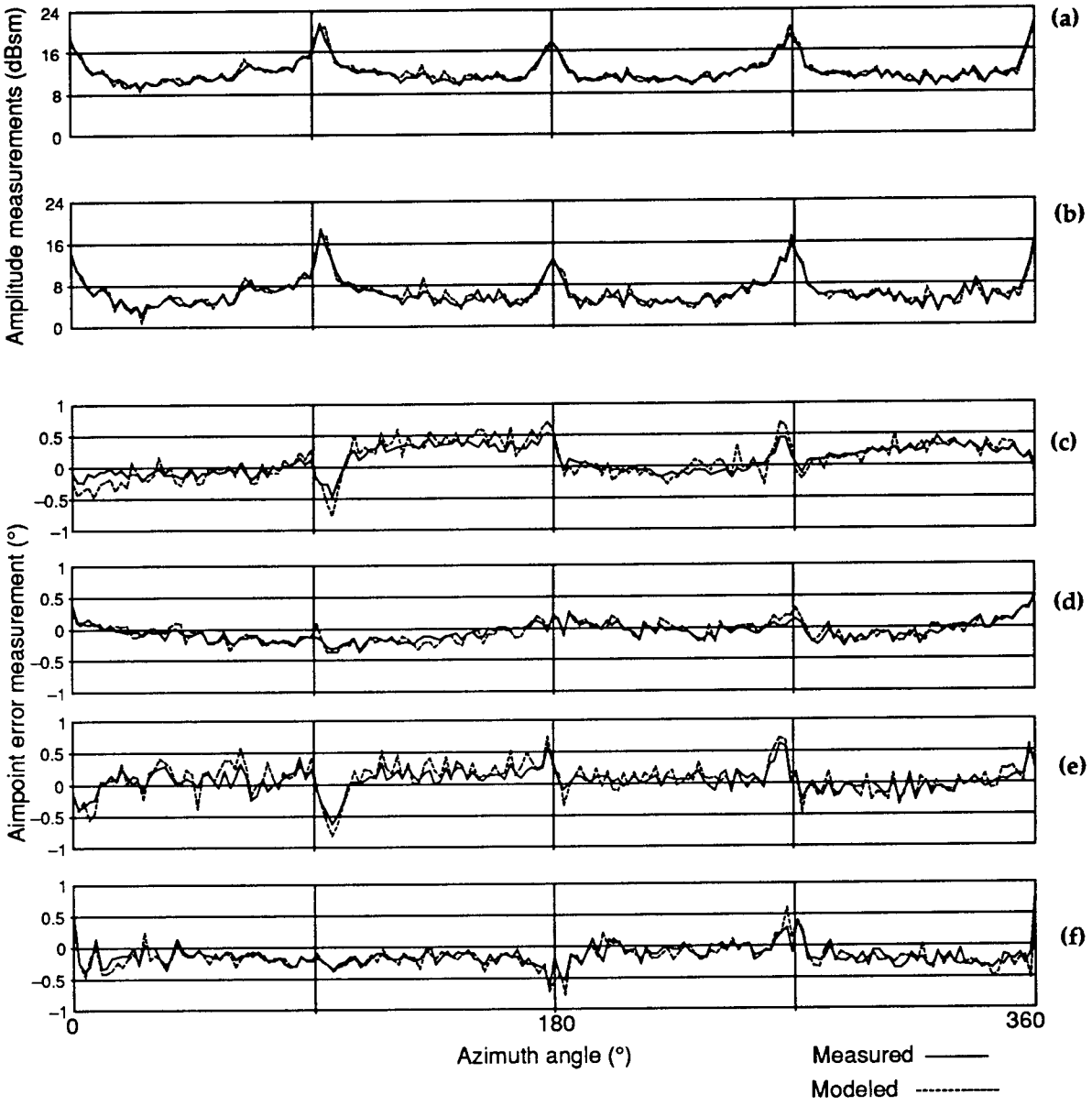

Figure 12. Measured and simulation RCS and aimpoint values smoothed with a 0.84° moving average window for a T-62 tank at a 60° radar depression angle: (a) RCS sum, (b) RCS peak, (c) azimuth aimpoint values for average algorithm, (d) elevation aimpoint values for average algorithm, (e) azimuth aimpoint values for peak algorithm, and (f) elevation aimpoint values for peak algorithm.

and plotted every 2°. At this level of resolution, the simulation curves track the measured curves with only a few minor deviations. The most noticeable deviations were from the azimuth aimpoint values. The simulation values appeared to have a slightly larger variance than the measured values.

The results of the quantitative analysis to determine the degree of agreement between measured and simulation RCS and aimpoint values for the full target are shown in table 2. The average and standard deviation of measured, simulation, and measured minus simulation values are listed in columns 2, 3, and 4. The standard deviation was computed after the values were smoothed over 1° azimuth intervals. The mean differences between measured and simulation values listed in column 4 are essentially zero for all calculations except for the peak RCS. The scatterer normalization procedure described in section 2.1 effectively guaranteed that the measured and simulation RCS values averaged over 360° were nearly equal; however, this procedure also resulted in larger simulation peak RCS values. The simulation peak RCS values were corrected for by the subtraction of an empirically calculated offset of 0.4 dB. This procedure was performed before the statistical tests were evaluated. If the scattering centers not incorporated into the target model had a random azimuth and elevation position on the target as it rotated with respect to the radar, then the average difference between the measured and simulation aimpoint values should also be equal to zero, as shown in column 4. These results confirm the basic properties expected for the model.

Further analysis of the results in table 2 show that the standard deviations of the measured values in column 2 are slightly smaller than those of the simulation values in column 3, with the average azimuth aimpoint calculation having the most noticeable difference. This may be the result of point scatterers creating greater interference patterns in the simulation of the radar returns than those normally created by imperfect scattering centers in measured radar returns. The measured and simulation standard deviations in columns 2 and 3 are considerably greater than the measured minus simulation standard deviations in column 4. This result indicates

Table 2. Full-target measured, simulation, and agreement results for a T-62 tank at 60° radar depression angle.

RCS and aimpoint position	Measured ave. ± std (dBsm or °)	Simulation ave. ± std (dBsm or °)	Agreement ave. ± std (dB or °)	Agreement KS test (% passed)	Agreement WSR test (% passed)
RCS sum	11.9 ± 2.2	12.0 ± 2.3	–0.04 ± 0.6	77	62
RCS peak	6.5 ± 2.7	6.9 ± 2.7	–0.40 ± 0.7	74	73
Azimuth average	0.09 ± 0.20	0.08 ± 0.26	0.01 ± 0.11	48	48
Elevation average	–0.07 ± 0.13	–0.07 ± 0.15	0.00 ± 0.07	52	52
Azimuth peak	0.05 ± 0.19	0.07 ± 0.21	–0.03 ± 0.11	52	77
Elevation peak	–0.16 ± 0.15	–0.17 ± 0.15	0.01 ± 0.10	46	82
Average	—	—	—	58	66

Note: agreement for KS and WSR tests was calculated at a 95-percent confidence level.

that the simulation RCS and aimpoint values tracked the measured values quite well.

The results of the KS and WSR tests are shown in columns 5 and 6 of table 2. The KS test average pass rate was 58 percent, and the WSR test average pass rate was 68 percent. The pass rates for the KS test are slightly lower and those for the WSR test slightly higher than those predicted by the results in figures 9, 10, and 11 (calculated for four 10° target azimuth intervals). This is probably a consequence of comparing results that contained a biased selection of high RCS target orientations, rather than the full target results. The KSR test pass rates were significantly higher for the peak azimuth and elevation aimpoint value results compared to the average azimuth and elevation aimpoint value results. This is not an unexpected result, since a single scattering center on the target may be responsible for many peak RCS and aimpoint values, which would be easier for a point scatterer model to simulate accurately than the average aimpoint values, which usually require multiple scattering centers. The results in table 2 are further analyzed in the next section.

3.4 Error Analysis

The precision of the measured and simulation values was separately analyzed as part of the evaluation of the model's performance. The precision of the measured RCS and aimpoint values was estimated from repeated radar measurements on the target, which were available for 9.4° between 45.8° and 55.2° azimuth. I evaluated the precision of the model by comparing simulation values calculated with target scattering centers having one selection of random position offsets to those calculated with identical target scattering centers having a different selection of random position offsets. This analysis was performed from 0° to 360° azimuth with the point scatterers selected by the 70-percent-scatterer selection criterion. The agreement between these measured values and the agreement between these simulation values were evaluated with the same criteria that were used to evaluate the model results.

Table 3. Quantitative analysis of precision measured and simulation RCS and aimpoint values.

RCS and aimpoint position	Precision of measurements ave. ± std (dB or °)	Precision of model ave. ± std (dB or °)	Agreement ave. ± std (dB or °)
RCS sum	–0.09 ± 0.17	0.02 ± 0.6	–0.04 ± 0.6
RCS peak	–0.03 ± 0.27	0.01 ± 0.7	–0.40 ± 0.7
Azimuth average	0.00 ± 0.03	0.00 ± 0.07	0.01 ± 0.11
Elevation average	0.00 ± 0.04	0.00 ± 0.06	0.00 ± 0.07
Azimuth peak	0.02 ± 0.07	0.00 ± 0.10	–0.03 ± 0.11
Elevation peak	–0.03 ± 0.06	0.01 ± 0.10	0.01 ± 0.10

Note: precision of measured values was evaluated for a 9.4° azimuth interval; precision and agreement of model were evaluated from 0° to 360° azimuth interval.

A quantitative analysis of the precision of measured and simulation values is shown in table 3. The average and standard deviation of the differences between measured minus measured values and simulation minus simulation values were computed for their respective full angular ranges (see eq (5)) and listed in columns 2 and 3 of table 3. The average values should converge to zero as the sample size becomes large. The near-zero results provide confidence in the correctness of the data acquisition system and the modeling software. Column 4 shows the agreement between measured and simulation values, which was previously computed and listed in table 2. These results were repeated so that the model's precision could be easily compared to its accuracy.

Analysis of standard deviation calculations in table 3 indicates that the lack of agreement between measured and simulation values was primarily caused by the lack of precision of the model-based calculations, not by target measurement error. A comparison of the standard deviations listed in column 2 to column 3 indicates that the precision of the measured values is about twice as high as that of the simulation values. The near-equal standard deviations in columns 3 and 4 indicate that the lack of agreement between the measured and simulation values is primarily caused by the random position offset associated with each scattering center. The only exception is the azimuth average aimpoint standard deviation, which I analyze further below.

A statistical analysis of the precision of measured and simulation values is shown in table 4. Columns 2 and 3 show the precision of measured values, columns 4 and 5 show the precision of simulation values, and columns 6 and 7 show the agreement between measured and simulation values, which was previously computed and shown in table 2. The KS and WSR tests were performed over 1° target azimuth intervals every 0.5°. A comparison of the percentage-passed rates in columns 2 and 3 to columns 4 and 5 indicates that the statistical reproducibility of the measured values was significantly better than that of the simulation values. The only exception was the average azimuth aimpoint pass rate for the KS test in column 2.

Table 4. Statistical analysis of precision of measured and simulation RCS and aimpoint values.

RCS and aimpoint position	Precision of measurements		Precision of model		Agreement	
	KS (% pass)	WSR (% pass)	KS (% pass)	WSR (% pass)	KS (% pass)	WSR (% pass)
RCS sum	100	88	75	71	77	62
RCS peak	94	94	78	67	74	73
Azimuth average	65	88	54	61	48	48
Elevation average	100	88	74	62	52	52
Azimuth peak	82	100	54	79	52	77
Elevation peak	94	100	54	77	46	82
Average	89	93	65	69	58	66

Note: precision of measured values was evaluated for a 9.4° azimuth interval; precision and agreement of model were evaluated from 0° to 360° azimuth interval; and agreement for KS and WSR tests was calculated at a 95-percent confidence level.

This lower value may have been caused by the aimpoint averaging algorithm being implemented with too low a threshold level. HRR cells with relatively low RCS would have relatively low signal-to-noise ratios (SNRs) and would therefore be more difficult to measure accurately, as was observed for the average azimuth aimpoint calculation. However, if this explanation is true, then the average elevation aimpoint calculation should also be more difficult to measure, which it is not. Since the difficulty arises in the average azimuth aimpoint calculation and not in the average elevation aimpoint calculation, it may be that the average azimuth angle calculation decorrelates faster for a target rotating in azimuth on a turntable. These factors could account for the lower average azimuth aimpoint percentage-passed rate, while having only a minimal effect on the azimuth peak and elevation average algorithm results. The results of the model probably could be more easily evaluated if a higher threshold level were chosen for the aimpoint averaging algorithm.

Examination of the percentage-passed rates associated with the precision of the model in table 4 indicates that the exact phase relationships between the scattering centers are important for determining RCS and aimpoint values. If a random position offset of less than a wavelength were unimportant, then the percentage-passed rates in columns 4 and 5 should all be approximately 95 percent. Obviously, this is not the case. This type of "random position offset" error is intrinsic to the point-scatterer model-based calculations; however, steps can be taken to minimize its effect. Slightly better agreement between measured and simulation values might have been achieved if each scattering center had been assigned a different random offset for every target orientation, rather than a random offset being assigned once to each set of target scattering centers and that set being rotated through several target orientations, as was done. For example, if two scattering centers were adjacent to each other, then a small change in target orientation would result in only a small change in phase relationships. This particular phase relationship could produce multiple constructive or multiple destructive interference patterns, which would probably not correspond with measurement-based calculations or other repeated model-based calculations. This would result in randomly biased calculations for the entire rotation interval. If a different random phase were assigned to each scattering center, there would be no tendency for the model to repeatedly produce slightly biased model-based calculations. Instead, there would be a greater chance of constructive or destructive interference patterns canceling over repeated calculations, producing simulation values that are closer to the measured values. This proposed change in the model could significantly increase the reproducibility of the model calculations and could slightly improve or at least not lessen the agreement between measurement- and model-based calculations.

A comparison of percentage-passed rates of the model's precision with its agreement (columns 4 and 5 with columns 6 and 7) shows that these are approximately equal for the WSR test and slightly lower for the KS test. Thus, the values near the median were probably modeled more accurately

than the outlying values. In view of this result, along with average azimuth aimpoint standard deviation results in table 3 and the visual analysis in section 3.3, a damping factor may need to be included in the target model to reduce the fluctuations in the simulation values. Further, the results in table 4 indicate that most of the statistical errors in the model-based calculations were also caused by the lack of precise information about the phase relationships between the scattering centers.

4. Conclusion

A simulation program based on the point-scatterer model was used to reconstruct 95-GHz, monopulse radar measurements of a T-62 Soviet tank taken with the target rotating on a turntable at a 60° radar depression angle. The agreement between measured and simulation RCS and aimpoint values was studied visually, quantitatively, and statistically. The precision of measured and simulation values was also studied. Most of this analysis was performed with 1° target azimuth intervals of processed data sampled every 0.5°. The tradeoffs between model validity and processing time were evaluated by the model being applied to progressively more complex target scattering center models over four 10° azimuth intervals of data. This analysis indicated that the agreement between simulation and measured values was asymptotically approaching a maximum level of validity, which could be achieved by the selection of scattering centers from a 3-D ISAR image that satisfied the 70-percent-scatterer selection criterion: the sum of the RCS of the selected scattering centers must contain at least 70 percent of the sum of the RCS of all the ISAR image resolution cells, and at least 40 scattering centers must be selected. Slightly higher model validity usually required an exponential increase in the number of scattering centers in the target model.

The target models were generated from 0° to 360° azimuth with the 70-percent-scatterer selection criterion. This criterion generated target models that had an average of 68 scatterers. Analysis of the model results indicated that agreement between measured and simulation RCS and aimpoint values was good visually and quantitatively, but mediocre statistically. Details are given in table 2. According to my analysis of the random errors associated with the measured and simulation values, measurement-based errors were usually small compared with model-based errors, and the model-based errors were about equal to the differences between the measured and simulation values. Thus, most of the discrepancies between measured and simulation values were caused by the lack of information on the exact phase relationships between scattering centers, rather than from poor measurement data, scattering centers decorrelating, or insufficient numbers of scattering centers. Overall, the visual and quantitative agreement between measured and simulated RCS and aimpoint values was good.

Acknowledgments

I would like to thank Jerry Silvious for his technical assistance in developing data unpacking subroutines and data processing subroutines; Joseph Nemarich for his guidance and editorial help; Herb Dropkin for many enlightening discussions on statistical analysis; and my colleagues who were responsible for collecting the T-62 tank radar data at Redstone Arsenal, Alabama.

References

1. K. R. Harrison, *Validation of Longbow Primary Test Vehicle Target Model,* Simulation Technologies, Inc., Tech Note 131-068 (1990).

2. A. V. Saylor and N. Evers, *Point Scatterer Model Development and Validation for 95 GHz T-62,* Simulation Technologies, Inc., Tech Note 131-108 (1992).

3. W. P. Yu, L. D. To, and K. Oh, *N-point Scatterer Model RCS/Glint Reconstruction from High-Resolution ISAR Target Imaging,* transcript from Pacific Missile Test Center, Point Mugu, California (1990).

4. J. C. Holtzman, J. A. Stiles, V. S. Frost, V. H. Kaupp, and E. E. Komp, *A Digital Computation Technique for Radar Scene Simulation: NEWS LAR,* Simulation (June 1979), 183–192.

5. R. J. Wellman, J. Nemarich, H. Dropkin, D. R. Hutchins, J. L. Silvious, and D. A. Wikner, *95-GHz Polarimetric Monopulse Radar Data for a T-62 Soviet Tank,* Harry Diamond Laboratories, special report for USA MICOM (February 1991).

6. R. J. Wellman, J. Nemarich, H. Dropkin, D. R. Hutchins, J. L. Silvious, and D. A. Wikner, *Polarimetric Monopulse Radar Scattering Measurements of Targets at 95-GHz,* NATO/AGARD Conference Proceedings 501 (September 1991), 30-1–31-13.

7. R. J. Wellman and J. L. Silvious, *Signal-Processing Techniques for Simulated Wideband Monopulse Radar Data,* Harry Diamond Laboratories, HDL-TR-2178 (1990).

8. D. R. Wehner, *High Resolution Radar,* Artech House, Inc., Massachusetts (1987), pp 341–368.

9. K. Vaccaro, *Point Scatterer Extraction Algorithm,* Pacific Missile Test Center, ITP-90-100 (February 1990).

10. J. S. Silverstein, *Down-Range Imaging of Radar Targets,* Harry Diamond Laboratories, HDL-TR-2166 (1990).

11. A. V. Saylor and K. R. Harrison, *Validation of Monopulse High Range Resolution Polarimetric Target Models,* Simulation Technologies, Inc., Tech Note 131-070 (October 1990), pp 3–4.

12. W. J. Conover, *Practical Nonparametric Statistics,* John Wiley & Sons, Inc., New York (1980), pp 280–281.

13. M. Hollander and D. A. Wolfe, *Nonparametric Statistical Methods,* John Wiley & Sons, Inc., New York (1973), pp 219–228.

Appendix. Generation of Monopulse Radar Antenna Patterns

The antenna patterns used in the simulation program and used for the beam shape correction of the inverse synthetic aperture radar (ISAR) images were constructed from ±3° azimuth and elevation scans of a dihedral reflector made with the Army Research Laboratory (ARL) instrumentation radar for right-hand transmitted, right-hand received (RR) polarization. The two-way 3-dB beam widths of the sum channel antenna pattern were measured to be approximately 2.3° in the azimuth and 2.0° in elevation. A simple algorithm was applied to interpolate the two scans into approximately circular antenna patterns for a full range of aspect angles as shown in

$$G_{sum}(\theta_{az},\theta_{el}) = \frac{S_{az}\left[\left(\theta_{az}^2+\theta_{el}^2\right)^{1/2}\right]}{S_{max\_az}}, \text{ if } |\theta_{az}|>|\theta_{el}| \text{ and } \theta_{az}>0, \quad (1)$$

$$G_{sum}(\theta_{az},\theta_{el}) = \frac{S_{az}\left[-\left(\theta_{az}^2+\theta_{el}^2\right)^{1/2}\right]}{S_{max\_az}}, \text{ if } |\theta_{az}|>|\theta_{el}| \text{ and } \theta_{az}\le 0,$$

$$G_{sum}(\theta_{az},\theta_{el}) = \frac{S_{el}\left[\left(\theta_{az}^2+\theta_{el}^2\right)^{1/2}\right]}{S_{max\_el}}, \text{ if } |\theta_{el}|>|\theta_{az}| \text{ and } \theta_{el}>0,$$

$$G_{sum}(\theta_{az},\theta_{el}) = \frac{S_{el}\left[-\left(\theta_{az}^2+\theta_{el}^2\right)^{1/2}\right]}{S_{max\_el}}, \text{ if } |\theta_{el}|>|\theta_{az}| \text{ and } \theta_{el}\le 0,$$

where $G_{sum}(\theta_{az},\theta_{el})$ = sum channel antenna pattern (in meters per meter), $S_{az}(\theta_{az})$ = sum channel measurements scanned in azimuth, $S_{el}(\theta_{el})$ = sum channel measurements scanned in elevation, S_{max_az} = maximum value of S_{az}, S_{max_el} = maximum value of S_{el}, θ_{az} = azimuth angle, and θ_{el} = elevation angle, with the optical geometric center of the target located at $\theta_{az} = 0°$ and $\theta_{el} = 0°$. The azimuth- and elevation-difference channel antenna patterns were obtained from $G_{sum}(\theta_{az},\theta_{el})$ multiplied by the measurements of the scanned ratios as shown in

$$G_{az}(\theta_{az},\theta_{el}) = G_{sum}(\theta_{az},\theta_{el})\mathrm{Re}\left[\frac{D_{az}(\theta_{az})}{S_{az}(\theta_{az})}\right],$$

$$G_{el}(\theta_{az},\theta_{el}) = G_{sum}(\theta_{az},\theta_{el})\mathrm{Re}\left[\frac{D_{el}(\theta_{el})}{S_{el}(\theta_{el})}\right],$$

where $G_{az}(\theta_{az},\theta_{el})$ = azimuth-difference antenna pattern (in meters per meter), $G_{el}(\theta_{az},\theta_{el})$ = elevation-difference antenna pattern (in meters per meter), $D_{az}(\theta_{az})$ = azimuth-difference channel measurements scanned in azimuth, $D_{el}(\theta_{el})$ = elevation-difference channel measurements scanned in elevation, $S_{az}(\theta_{az})$ = sum channel measurements scanned in azimuth, and $S_{el}(\theta_{el})$ = sum channel measurements scanned in elevation.

Distribution

Admnstr
Defns Techl Info Ctr
Attn DTIC-DDA (2 copies)
Cameron Sta Bldg 5
Alexandria VA 22304-6145

Director
Advncd Rsrch Proj Agcy Archt Bldg
Attn Target Acqstn & Engagement Div
3701 N Fairfax Dr
Arlington VA 22203-1714

Under Secy of Defns for Rsrch & Engrg
Attn Rsrch & Advncd Tech
Depart of Defns
Washington DC 20301

CECOM NVESD
Attn AMSEL-RD-NV-ASD M Kelley
Attn Techl Lib
Attn AMSEL-RD-NV-VISPD T Witten
FT Belvoir VA 22060

Commander
US Army Armament RDE Ctr
Attn SMCAR-FSP-A1 M Rosenbluth
Attn SMCAR-FSP-A1 R Collett
Picatinny Arsenal NJ 07806-5000

US Army CECOM
Attn AMSEL-RD-NV-RSPO A Tarbell
Mailstop 1112
FT Monmouth NJ 07703-5000

US Army Materiel Cmnd
Attn AMCDM Dir for Plans & Anlys
5002 Eisenhower Ave
Alexandria VA 22333-0001

Director
US Army Matl Sys Anlys Actvty
Attn AMXSY-MP
Aberdeen Proving Ground MD 21005-5066

US Army Mis Lab
Attn AMSMI-RD Advncd Sensors Dir
Attn AMSMI-RD Sys Simulation & Dev Dir

US Army Mis Lab (cont'd)
Attn AMSMI-RD-AS-MM G Emmons
Attn AMSMI-RD-AS-MM M Mullins
Attn AMSMI-RD-AS-MM S Mobley
Attn AMSMI-RPR Redstone Scntfc Info Ctr
Attn AMSMI-RD-SS J Cole
Attn AMSMI-RD-AS-MM M Christian
Attn AMSMI-RPT Techl Info Div
Redstone Arsenal AL 35809

US Army Test & Eval Cmnd
Attn STEWS-TE-LG S Dickerson
Attn STEWS-TE-AF F Moreno
White Sands Missile Range NM 88002

Director
Nav Rsrch Lab
Attn 2600, Techl Info Div
4555 Overlook Ave SW
Washington DC 20375

Commander
Nav Surfc Weapons Ctr
Attn E-43 Tech Lib
White Oak MD 20910

Naval Surfc Weapons Ctr
Attn DX-21 Lib Div
Dahlgren VA 22448

Nav Weapons Ctr
Attn 38 Rsrch Dept
Attn 381 Physics Div
China Lake CA 93555

Dept of the Air Force, HQ
Radar Target Scatter Facility
Attn LTC R L Kercher Chief
6585th Test Grp (AFSC)
Holloman AFB NM 88330

Sandia Natl Lab
PO Box 5800
Albuquerque NM 87185

Distribution

Environ Rsrch Inst of MI
Attn IRIA Lib
PO Box 618
Ann Arbor MI 48107

Georgia Tech Rsrch Inst
Georgia Inist of Techlgy
Attn Radar & Instrmntn Lab T L Lane
Atlanta GA 30332

Lincoln Lab Massachusetts Inst of Techlgy
Attn R M Barnes
Lexington MA 02173

Simulation Technologies Inc
Attn A V Saylor
PO Box 7009
Huntsville AL 35807

TASC
Attn K L Weeks
907 Mar-Walt Dr
FT Walton Beach FL 32548

US Army Rsrch Lab
Attn AMSRL-WT-WB R A McGee
Aberdeen Proving Ground MD 21005

US Army Rsrch Lab
Attn AMSRL-OP-SD-TA Mail & Records Mgmt
Attn AMSRL-OP-SD-TL Tech Library (3 copies)

US Army Rsrch Lab (cont'd)
Attn AMSRL-OP-SD-TP Tech Pub
Attn AMSRL-SS J Sattler
Attn AMSRL-SS-I J Pellegrino
Attn AMSRL-SS-S E Burke
Attn AMSRL-SS-S J M Miller
Attn AMSRL-SS-SD B Wallace
Attn AMSRL-SS-SD D Hutchins
Attn AMSRL-SS-SD D W Vance
Attn AMSRL-SS-SD D Wikner
Attn AMSRL-SS-SD G Goldman (20 copies)
Attn AMSRL-SS-SD J Silverstein
Attn AMSRL-SS-SD J Silvious
Attn AMSRL-SS-SD K Tom
Attn AMSRL-SS-SD P Cremona-Simmons
Attn AMSRL-SS-SD R Wellman
Attn AMSRL-SS-SG J Sichina
Attn AMSRL-SS-SH J Nemarich
Attn AMSRL-SS-SH Z G Sztankay
Attn AMSRL-SS-SD H Dropkin
Attn AMSRL-SS-SJ M Hamilton